Evolution of the structural and bonding properties of aluminum-lithium clusters

S. Chacko* and D. G. Kanhere†
Center for Modeling and Simulation and Department of Physics, University of Pune, Pune 411 007, India

V. V. Paranjape
Department of Physics, Lakehead University, Thunder Bay, Ontario, Canada P7B 5E1
(Received 15 September 2003; published 25 August 2004)

We report a detailed study of the electronic structure, energies, and the nature of bonding in various Al -Li clusters: Al_nLi_n($n=1-11$), Al_2^-, Al_2^{2-}, Al_2Li, Al_2Li^-, and Al_6Li_8. We use the standard Born-Oppenheimer molecular dynamics within the framework of density-functional theory. The growth structure in these clusters is found to occur in two broad categories: the first (for $n=2-4$) has the structure of a bent rhombus, and the second ($n=7-9,11$) has the structure of a pentagonal ring. A substantial charge transfer between the atoms is observed in nearly all the clusters with the exception of Al_2Li_2. In this cluster, a hybridization of the 2*s* orbital of Li with the 3*p* orbital of Al is observed. In clusters with more than six Al atoms, the eigenvalue spectrum is divided into two main groups: at the lower end of the energy spectrum, jelliumlike orbitals are observed, while at the higher end, localized bonds are seen. The localized bond formation appears to result from the interaction between *p* electrons on each of the Al atoms. We also have found a tetravalent structure for Al atoms within the Al-Li cluster arising due to a charge transfer from the Li atoms to the Al atoms.

DOI: 10.1103/PhysRevA.70.023204 PACS number(s): 36.40.−c, 31.15.−p, 61.46.+w, 73.22.−f

I. INTRODUCTION

There has been considerable research activity in the field of cluster physics following the discovery of C_{60} buckminsterfullerene [1], observation of magicity in metallic clusters [2], unusual thermodynamical properties of clusters of atoms like Na [3], Sn [4], etc. Theoretical and experimental [5–7] studies have been carried out extensively to understand the physical and chemical properties of clusters which include structural and electronic properties, the nature of bonding, thermodynamics, vibrational, and rotational properties. The gradual emergence of the bulk properties as the cluster size is increased has also attracted much attention.

Aluminum-lithium clusters, which we study in this paper, have interesting structural and bonding properties and both exhibit an interplay between aluminum and lithium atoms. These properties are quite different from those of the pure clusters of the constituent elements. We have selected Al_nLi_n clusters with a moderate number of aluminum and lithium atoms where the number of atoms of each element does not exceed 11. We have also included in our study Al_2 clusters which contain uncompensated electronic charges. Since the number of atoms in all the clusters is sufficiently low, we have been able to employ a powerful numerical technique based on the Born-Oppenheimer molecular dynamics (BOMD) [8] within the density-functional theory (DFT). The numerical procedure consists of using the classical equations of motion, for a short time step, on the randomly selected atomic positions with velocities appropriate to a given temperature. The force on each of the atoms is provided by the electrons whose charge distribution is given by DFT. The process is repeated until the energy minimum for the atomic positions is realized. The procedure provides a reasonably accurate method for determining the atomic and electronic structures for the clusters studied in this paper.

Both pure Al and Li clusters have been extensively studied using the spherical jellium model (SJM) [2]. It is known that the SJM is quite successful in describing the gross electronic structure and stability of alkali-metal clusters [2,9]. SJM is, however, not sufficiently reliable to predict fully properties of Al clusters. Rao and Jena [10] have reported a comprehensive study of the aluminum clusters using *ab initio* density-functional theory. The DFT, used by several authors, is certainly a more accurate method than SJM, but it still does not provide as detailed a structural simulation as the method based on molecular dynamics, which we use. Rao and Jena found that in Al clusters with a small number of atoms, the effective valency of Al is unity [10]. This is due to a large energy gap of about 5 eV separating the $3s^2$ and $3p^1$ orbitals. This conclusion was later contradicted by Rao *et al.* [11] and Dhavale *et al.* [12]. Investigation by Cheng *et al.* [13] shows that a single Al atom in Li clusters introduces a localized bond between the Al impurity and the Li host. They also found that $AlLi_5$ is a magic cluster and suggested that Al_nLi_{5n} might also be magic for at least some of the values of $n \geqslant 2$. Akola *et al.* [14], however, found that this idea does not apply beyond $n=2$. Further, their investigations on bonding in Li-rich Al-Li clusters show that a substantial charge transfer occurs from Li atoms to the Al atoms. This leads to the strengthening of the ionic nature of the Al -Li bond, and also the Al-Al covalent bond. Such a charge transfer has also been observed by Kumar [15] in several mixed Al-Li clusters. He found a layered $Al_{10}Li_8$ compound to be magic with closure of the electronic and geometric shell. This was the first instance where a shell closure in an *s-p* bonded metal-atom cluster was found to occur at 38 valence electrons. This does not agree with the magic numbers

*Email address: chacko@physics.unipune.ernet.in
†Email address: kanhere@unipune.ernet.in

for alkali-metal clusters [2], which are 2, 8, 18, 20, 40, etc., and the magic Al clusters: Al_7^+, Al_7^-, Al_{11}^-, Al_{13}^-, etc. [10,16].

Recently observed aromaticity [17] and antiaromaticity [18–21] in inorganic molecules, and in particular Al-Li clusters, has stimulated research in these systems. These properties are well-known and important in organic chemistry [22]. While aromaticity and antiaromaticity are not a uniquely defined concept theoretically, experimentally they are detected by measuring external magnetic-field-induced *ring currents*. The first experimental and theoretical evidence of aromaticity in an all-metal system, viz., Al_4^{2-} and MAl_4^- (M=Li, Na, Cu), was recently given by Wang and co-workers [17]. They found that the Al_4^{2-} dianion has a square-planar structure possessing two π electrons, which is considered to be the structural criterion for aromaticity. The concept of antiaromaticity, introduced by Breslow *et al.* [23], corresponds to the destabilization as seen in the cyclic systems with $4n$ π-electrons. Although such molecules have not yet been observed except in organic chemistry, calculations reported by Shetty *et al.* [18,20] and others [21] indicate, using Breslow's criterion [23], that the Al_4Li_4 cluster is antiaromatic. We have also examined these properties for Al-Li clusters.

The Al-Li bulk is especially interesting due to the fact that it forms a stable alloy over a wide range of concentrations. However, the most stable intermetallic B32 phase corresponds to the 50:50 concentration [24]. The stability, interestingly, even includes clusters with a small number of atoms, as noted in this paper. In the B32 phase, a mixture of covalent and ionic bonding is observed due to a charge transfer from the Li atoms to the Al atoms. Moreover, the density of states (DOS) of this phase (without any band gap) [25] shows a close resemblance to that of the covalently bonded diamond structure. Thus, based on these observations, one may expect that the behavior of Al in Al_nLi_n would be similar to that of tetravalent atoms such as Si [26], Ge [27], Sn, and Pb [28]. Indeed, our present work shows that in some of the clusters, the structure and bonding of Al_n is similar to that of the group IV–A clusters. Moreover, earlier work [10–15] on the heterogeneous Al-Li clusters has focused on specific aspects such as geometry, stability, shell closure, magic behavior, etc. Bonding in such clusters was discussed on the basis of total charge density as well as the difference of the self-consistent charge density (ρ_{SCF}) and the superimposed atomic charge densities ($\rho_{superimposed}$) of the constituent atoms. However, analysis of the molecular orbitals (MOs) has revealed some unusual properties, such as aromaticity and antiaromaticity in all-metal Al-Li clusters. In our earlier work, we have examined some of the issues concerning the geometry and the stability of various Al-Li clusters, viz., Al_nLi_n (n=1–10,13) [29], Al_nLi_7 (n=1–7) [30], $AlLi_n$(n=1,8) [30], and $Al_{13}Li_n$(n=1–4,10,19,20,21) [33]. We found that the geometries of these clusters were determined by the geometry of the core Al cluster, enclosed in a Li cage. However, since these calculations were performed by density-based molecular dynamics (DBMD), analysis of the bonding and electronic structure could not be performed. In the present work, we study, using a more powerful numerical technique based on BOMD, the geometries, energies, electronic structure, and bonding properties in various Al-Li clusters, viz., Al_nLi_n(n=1–11), Al_2^-, Al_2^{2-}, Al_2Li, Al_2Li^-, and Al_6Li_8 within the pseudopotential and the generalized gradient approximation (GGA). The bonding in these clusters is analyzed via the electron localization function (ELF) [32] and the molecular orbitals. In Sec. II, we shall describe the computational details, followed by a discussion of the results in Sec. III.

II. COMPUTATIONAL DETAILS

The ground-state geometries as well as other low-energy structures were obtained in two stages. In the first stage, Born-Oppenheimer molecular dynamics [8] based on Kohn-Sham (KS) [33] formulation of density-functional theory was employed. The computer code used for this purpose was developed in our group. The total energy during each of the molecular-dynamics steps was minimized using the damped equation of motion [34]. The calculations were performed using the norm-conserving pseudopotentials of Bachelet *et al.* [35] in the Kleinman-Bylander [36] form with the *s* part treated as nonlocal. The exchange-correlation potential was calculated using the local-density approximation (LDA) given by Ceperley and Alder [37]. A cubic supercell of length 40 a.u. with an energy cutoff of $\approx$17 Ry was found to provide sufficient convergence of the total energy. Increasing the energy cutoff did not change the total electronic energy significantly.

The damped equation of motion scheme [34] permits use of a fairly moderate time step $\approx$2.2 fs. Starting from a random configuration, the Al_nLi_n clusters were heated to 1400–1700 K and allowed to span the phase space for a few thousand iterations. In our previous investigations [29–31] on Al-Li clusters, it was found that the Li atoms segregate at the surface with the Al atoms forming an inner core. In order to avoid any such segregation, during the molecular-dynamics run we have interchanged the Al and the Li atoms. This has ensured that the cluster visits all its local minima as well as the global minimum. At the end of each ionic displacement, the norm of the eigenstates defined as $|h\psi_i - \epsilon_i\psi_i|^2$ (where ϵ_i is an eigenvalue corresponding to the eigenstate ψ_i of the Kohn-Sham Hamiltonian h) was within the range of 10^{-4}–10^{-7} a.u.

In the second stage, various low-energy structures were obtained by the conjugate gradient and/or steepest descent [8] method starting from various suitable configurations during the molecular-dynamics run. These configurations were then optimized using ultrasoft pseudopotentials [38] within the generalized gradient approximation (GGA) implemented in the VASP [39] package. The Perdew-Wang [40] exchange-correlation potential for GGA has been used. The size of the simulation cell was varied according to the cluster studied (see Table I).

The geometries were optimized with a kinetic-energy cutoff of the order of $\approx$12 Ry. This energy cutoff was sufficient for the convergence of the total energy. Increasing the energy cutoff did not change the total electronic energy significantly. The structures were considered to have converged when the forces on each ion were less than 0.01 eV/Å with a convergence in the total energy within the range of 10^{-4}–10^{-6} eV.

TABLE I. Size of the supercell (in Å) for various clusters, where n is the total number of atoms in the clusters.

n	Simulation cell (Å)
2,4,6	$16\times16\times16$
8,10,12	$18\times18\times18$
14,16.18,20	$20\times20\times20$

In general, we find that there are many isomeric structures nearly degenerate to the lowest-energy state. Few of the structures can be obtained by interchanging the Al and the Li atoms or by rearranging the position of Li atoms. In the present work, we discuss only a few geometries close to and at the lowest energies.

The nature of the bonding has been investigated via the electron localization function (ELF) [32], the molecular orbitals (MO), and the charge-density difference (ρ_{SCF} -$\rho_{\mathrm{Superimposed}}$, as defined earlier). The ELF has been found to be more reliable for elucidating the bonding characteristics of clusters, especially in conjunction with the charge density. The value of the ELF lies between 0 and 1, and a value of 1 represents a perfect localization of the valence charge.

III. RESULTS AND DISCUSSION

A. Structure, energies, and stability

The geometrical structures for the ground and the low-lying energy states for Al_nLi_n clusters, obtained using BOMD, are shown in Fig. 1 for $n=2-6$ and Al_6Li_8, while in Fig. 2 for $n=7-11$. The stability is discussed via the binding energy (E_b), the dissociation energy (ΔE), and the second-order difference in the total energy with respect to a single Al-Li pair (Δ^2E), and the energy gap between the highest occupied molecular orbital (HOMO) and the lowest unoccupied molecular orbital (LUMO). These quantities are defined by the expressions

$$E_b[\mathrm{Al}_n\mathrm{Li}_n] = \{-E[\mathrm{Al}_n\mathrm{Li}_n] + n(E[\mathrm{Al}] + E[\mathrm{Li}])\}/2n,$$

$$\Delta E[\mathrm{Al}_n\mathrm{Li}_n] = (E[\mathrm{Al}_n\mathrm{Li}_n] - E[\mathrm{Al}_{n-1}\mathrm{Li}_{n-1}]) - E[\mathrm{Al\ Li}],$$

$$\Delta^2E[\mathrm{Al}_n\mathrm{Li}_n] = (E[\mathrm{Al}_{n-1}\mathrm{Li}_{n-1}] - 2E[\mathrm{Al}_n\mathrm{Li}_n]) - E[\mathrm{Al}_{n+1}\mathrm{Li}_{n+1}],$$

where $E[\mathrm{Al}_n\mathrm{Li}_n]$ is the total energy of the Al_nLi_n cluster. We have plotted (E_b) in Fig. 3(a) and ΔE, Δ^2E in Fig. 3(b) for Al_nLi_n clusters for the values of n from 1 to 11. In Fig. 3(c), we show the variation in the energy gap (HOMO-LUMO) for $n=1-11$. Clearly, a pronounced maximum in the dissociation energy (ΔE) along with a corresponding minimum in Δ^2E signifies the cluster stability. We have also plotted in Fig. 3(d) the smallest distance between Al-Al, Al-Li, and Li-Li as a function of n.

The ground-state structure of Al_2Li_2 is a bent rhombus [Fig. 1(a), (1)], while a planar geometrical structure [Fig. 1(a), (2)] is seen for a low-energy state of Al_2Li_2. The bent rhombus structure of Al_2Li_2 is found to be one of the stable structure of all structures of Al_nLi_n studied in this paper. A

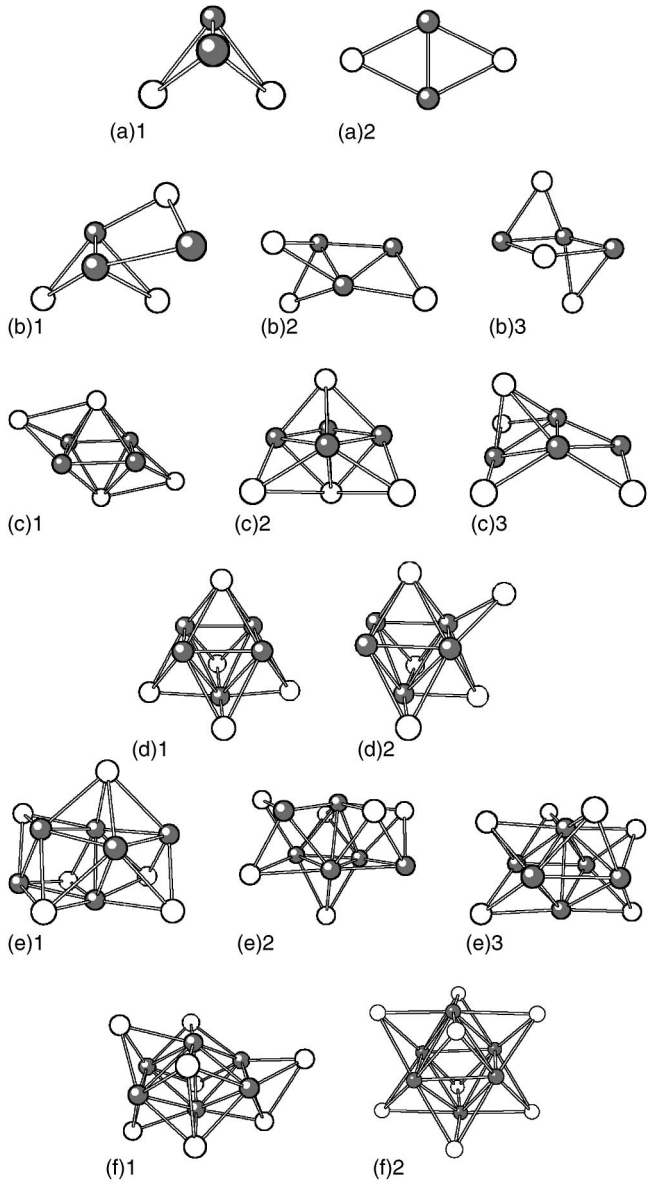

FIG. 1. The ground state and the low-energy geometries of the $Al_nLi_n(n=2-6)$ and Al_6Li_8 clusters. The black circles represent Al atoms and the white circles represent Li atoms. The lowest-energy structure is represented by (1).

substantial rise in the binding energy [Fig. 3(a)] is observed when two Al-Li dimers combine to form Al_2Li_2 cluster. A peak in the dissociation energy (ΔE) [Fig. 3(b)], a minimum in the second difference in energy (Δ^2E) [Fig. 3(b)], and a rather large HOMO-LUMO gap [Fig. 3(c)] signify a relatively high stability of this cluster. Interestingly, the planar Al_2Li_2 structure, with some bending, has been observed by Kumar [15] within the magic cluster $Al_{10}Li_8$. However, because of the restricted nature of his numerical procedure, he did not find stability for this eight valence-electron system.

A bent rhombus structure is also seen for the ground states of Al_3Li_3 and Al_4Li_4 [Figs. 1(b), (1) and 1(c), (1)]. The Al_3Li_3 cluster is not energetically as stable as Al_2Li_2, as can be deduced from Figs. 3(a)–3(c). The ground-state structure of Al_4Li_4 is found to be formed by the combination of two

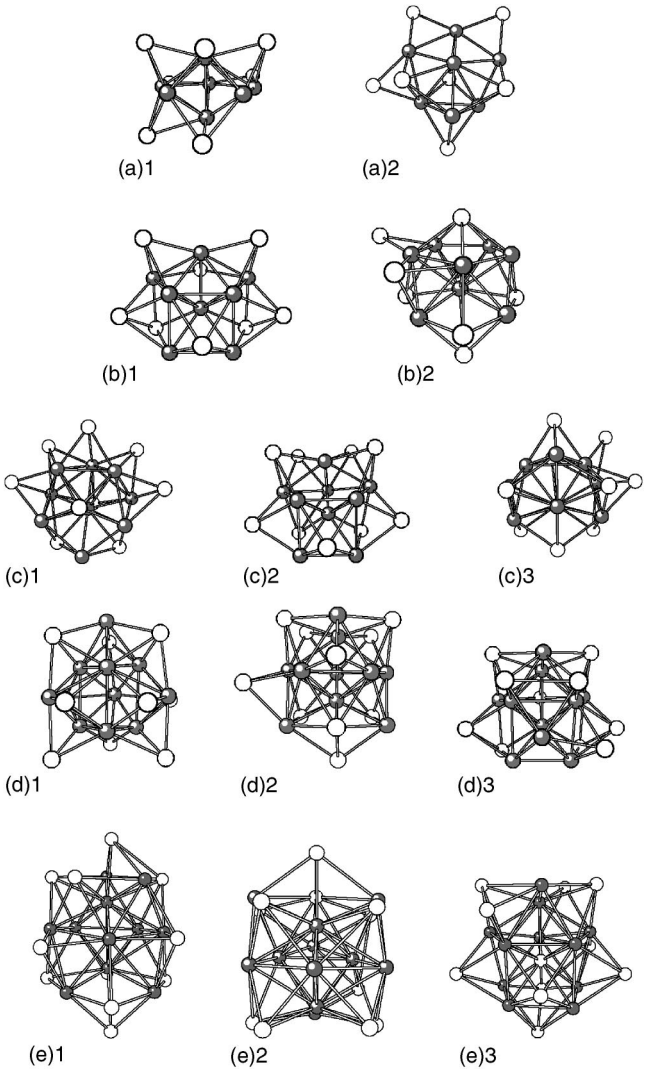

FIG. 2. The ground state and the low-energy geometries of the $Al_nLi_n (n=7-11)$ clusters. The black circle represents Al atoms and the white circles represent Li atoms. The lowest-energy structure is represented by (1).

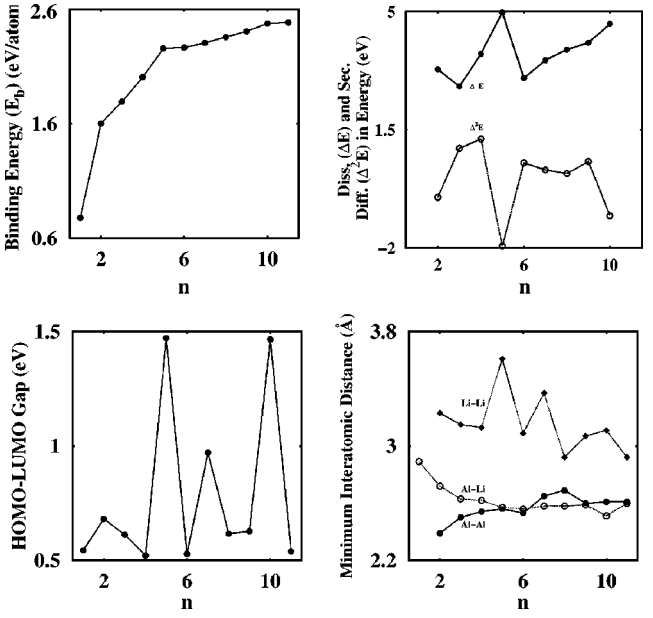

FIG. 3. (a) The binding energy per atom (in eV/at) of the Al_nLi_n cluster ($n=1-11$). (b) The dissociation energy (ΔE) and the second difference in the total energy ($\Delta^2 E$) of the Al_nLi_n clusters ($n=2-10$) with respect to an Al-Li dimer. (c) The HOMO-LUMO gap (in eV) in the Al_nLi_n cluster ($n=1-11$). (d) The minimum interatomic distance Al-Al, Al-Li, and Li-Li (in Å) in the Al_nLi_n cluster ($n=1-11$).

units of Al_2Li_2 [Fig. 1(c), (1)]. The two units are arranged to form a rectangle out of the four Al atoms. Indeed, it is this rectangular shape, studied by our group [18,20,41] and others [21], that gives rise to an antiaromatic property to this cluster [18,21]. The two low-energy structures of Al_4Li_4 [Figs. 1(c), (2) and 1(c), (3)] have two distinct forms: a square-plane and a bent rhombus formed out of four Al atoms, respectively.

The structure of Al atoms in Al_4Li_4 and in Al_5Li_5 is distinctly different. In Al_4Li_4 the Al atoms lie on a single plane and occupy the four corners of a rectangle while in Al_5Li_5 the structure becomes three-dimensional: the four atoms form a square-plane and the fifth atom lies above the plane to coincide with the center of the square. The latter structure, therefore, resembles a pyramid. Dhavale *et al.* have reported a similar pyramidal structure for Al_5Na_5. It is of interest to compare the structure of aluminum in pure Al_4 and Al_5 clusters with the corresponding structure for aluminum in Al_4Li_4 and Al_5Li_5. Aluminum in Al_4 shows a planar geometry with a rhombus structure. However, in Al_5 the growth of aluminum occurs in a plane and does not follow the three-dimensional growth seen in Al_5Li_5. In fact, the three-dimensional structure in pure Al_n cluster is seen only when n exceeds 5. We also find that the Al_5Li_5 cluster forms the most stable structure among the clusters studied in this paper. The stability follows after examining the binding energy, ΔE, $\Delta^2 E$, and the HOMO-LUMO gap from Figs. 3(a)–3(c). Another interesting feature of the Al_5Li_5 cluster is that it shows the formation of a plane composed of four Li atoms at the corners of a square with an Al atom at its center. The planar structure resembles, but is not identical to, the face of a fcc cell. A complete fcc structure is formed in an Al_6Li_8 cluster, with six Al atoms at the face-centered sites and eight Li atoms at the vertices of the cube, as deduced by Shah *et al.* [29] using DBMD. These authors find the Al_6Li_8 structure to be of the lowest energy. We, on the other hand, find that the fcc structure is not of the lowest energy. In Fig. 1(f), (1) and (2), we show both the lowest energy and the fcc structures, respectively, and conclude that the fcc structure (with some distortion) is 1.11 eV higher in energy than the ground state. We also observe that in the series Al_4^{2-}, Li-Al_4^-, Al_5Li_5, and Al_6Li_8, a three-dimensional octahedral growth of an Al cluster is enclosed in a cage formed by Li atoms and leads to an effective delocalization of the electron density (see Sec. III B).

The Al_6Li_6 cluster shows a geometry similar to that of Al_5Li_5, with distortions in the Al_4 square-plane [Fig. 1(e), (1)]. In the first low-energy structure [Fig. 1(e), (2)], a tetrahedra of Al_4 is seen, while the other low-energy structure [Fig. 1(e), (3)] shows an octahedra of Al_6. The octahedral

structure is also known to be the ground-state geometry of a pure Al_6 cluster [10].

The appearance of a pentagonal ring, which is a precursor to the icosahedral growth, is seen for $n=7$ (Al_{13} is a distorted icosahedron in its ground state [42]). The ground-state geometry of Al_7Li_7 shows a pentagonal bipyramid which is capped by the Li atoms [Fig. 2(a), (1)]. The appearance of a similar pentagonal ring in pure Al clusters (in neutral as well as singly charged form) is seen for Al_9 [10], as well as in tetravalent atom clusters such as Sn and Pb [28] for seven-atom clusters. Incidentally, these clusters are isoelectronic to Al_7Li_7 with 28 valence electrons. The low-energy structure of Al_7Li_7 [Fig. 2(a), (2)] as well as the ground-state geometries of $n=8$, 9, and 11 clusters [Figs. 2(b), (1); 2(c), (1); and 2(e), (1); respectively] also exhibit such pentagonal rings. However, the lowest-energy structure of the $Al_{10}Li_{10}$ cluster [Fig. 2(d), (1)] is different from that of the Al_7Li_7 to Al_9Li_9 and $Al_{11}Li_{11}$, with respect to the fact that no evidence of the pentagonal ring is seen. In fact, the geometry of Al_{10} in $Al_{10}Li_{10}$ is similar to that of Sn_{10}, i.e., a tetracapped trigonal prism (TTP) [43] with some mild distortions. The $Al_{10}Li_{10}$ cluster shows magical behavior since it exhibits a peak in the dissociation energy (ΔE), a minima in the second difference in energy ($\Delta^2 E$), and a large HOMO-LUMO gap [Figs. 3(a)–3(c), respectively].

We have performed analysis of the interatomic bond distances in order to understand the mixing and segregation behavior of the Al and the Li atoms. In Fig. 3(d), we plot the smallest bond distances of Al-Al, Al-Li, and Li-Li as a function of the number of Al atoms in the Al_nLi_n cluster. We find that in clusters with a smaller number of atoms ($n \leqslant 4$), the Al-Al bond is stronger than other bonds. However, from $n \geqslant 5$, the Al-Li bond distance becomes comparable to that of Al-Al. We recall that for $n \geqslant 5$, the Al_n structure becomes three-dimensional, which gives rise to an increase in the surface area. This allows the Li atoms to maximize the number of Al-Li bonds and brings Li atoms closer to the Al atoms.

It is well known that the density-based method (DBMD) is not as accurate as the Kohn-Sham approach (BOMD), nonetheless it has been extensively used to investigate the geometry and stability of various Al-Li clusters [29–31]. Here, we make some pertinent comments on the difference in the geometry of the Al_nLi_n clusters obtained by these two methods. Our results show that the geometries of some of the clusters were in good agreement with those predicted by DBMD. For instance, the structure of Al_2Li_2 was found to be a bent rhombus by both methods (see Ref. [29] for DBMD results). The geometries of other clusters such as Al_7Li_7 to Al_9Li_9 are nearly similar to those obtained by DBMD. However, there are clusters where the geometries are quite different from those given by the BOMD method. For instance, the structure of Al_3Li_3 predicted by DBMD is a capped trigonal bipyramid [29]. Using BOMD, the same structure gets Jahn-Teller distorted into a structure with a bent rhombus of Al_2Li_2. The evolution in the geometry by the DBMD method shows an earlier appearance of a three-dimensional structure of Al_n at $n=4$ (Al_4 is a tetrahedra in Al_4Li_4), while a planar structure is observed using BOMD. A three-dimensional pyramidal structure of Al_5 in Al_5Li_5 is observed by us.

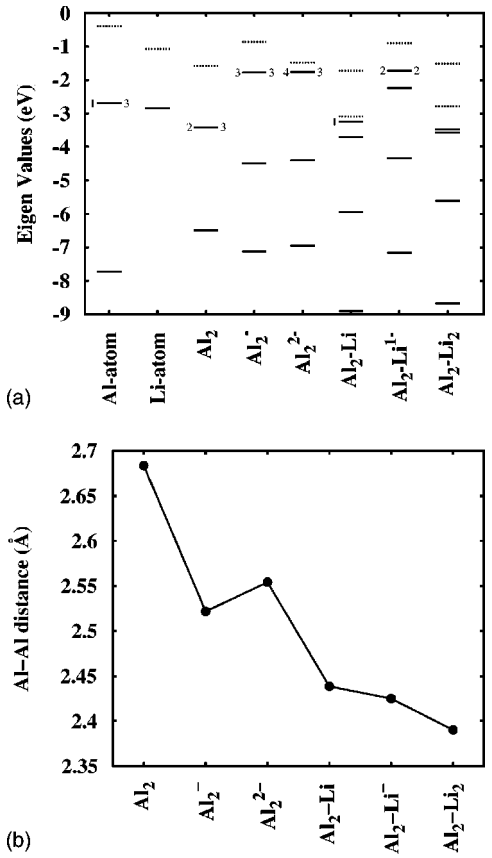

FIG. 4. (a) The eigenvalue spectrum (in eV). The continuous lines correspond to occupied orbitals and dashed lines correspond to the empty orbitals. The numbers on the right indicate the degeneracy of the orbitals. The numbers on the left indicate the occupancies of the orbitals. All other occupied orbitals have two electrons. (b) The Al-Al bond distance (in Å).

B. Bonding

1. Al_2Li_2

As noted earlier, Al_2Li_2 is one of the stable clusters. It has eight valence electrons, which correspond to a closed shell in the jellium model. However, the behavior of the MOs as well as the eigenvalue spectrum, obtained by us, does not support the conclusions of SJM. Kumar [15] found that the bonding between Al-Li in the planar Al_2Li_2 structure is ionic. On the contrary, our investigation with the bent rhombus structure in Al_2Li_2 shows insignificant charge transfer from the Li atoms to the Al atoms. The analysis based on the charge-density difference, however, shows that a charge transfer from the Li atoms to the bonding region between the Al and Li atoms does take place (figure not shown). In order to get better insight into the bonding properties in Al_2Li_2, we have studied Al_2, Al_2^-, Al_2^{2-}, Al_2Li, Al_2Li^-, and Al_2Li_2 clusters. This series represents a growth of Al_2Li_2 starting from the Al_2 dimer. In Fig. 4, we show the eigenvalue spectrum, as well as the Al-Al bond distance for the optimized geometries for these clusters. The eigenvalue spectra of Al_2 [Fig. 4(a)], in neutral, singly, and doubly charged forms, show a triply degenerate HOMO. These orbitals are partially filled and are described in terms of two π bonds and one σ bond (figure

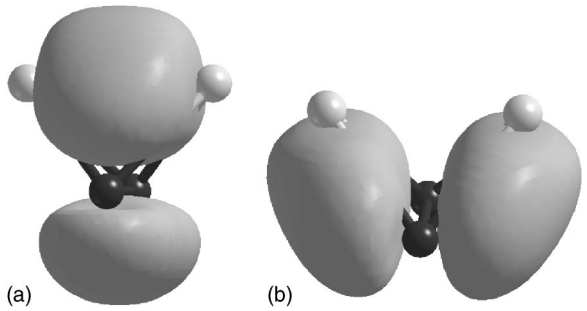

FIG. 5. The isodensity surface of the second highest-energy occupied orbital and the highest occupied molecular orbital of Al_2Li_2 at one-fifth of its maximum value. The black circles represent Al atoms and the gray circles represent the Li atoms.

not shown). Successive substitution of electrons by Li atoms splits the HOMO, thus reducing the degeneracy. In both cases, the *s* orbital of the Li atom hybridizes with the *p* orbital of the Al atom. In Fig. 5, we show the second highest-energy occupied molecular orbital and the HOMO of the Al_2Li_2 cluster. Clearly, these orbitals show the *sp* hybridization of the 3*p* orbital of Al with the 2*s* orbital of the Li atoms. In Fig. 4(b), we also plot the Al-Al bond distance in these clusters. A contraction of the Al-Al bond upon addition of either an electron or a Li atom is seen. The contraction of the bond with the addition of a Li atom is more pronounced than that with the addition of an electron. This might be due to the hybridization. Thus, the enhanced stability of Al_2Li_2 may be attributed to the *sp* hybridization in this cluster.

2. Al_4Li_4

The bonding in the Al_4Li_4 cluster has been studied extensively by us [18,20,41] and others [21]. The cluster has been found to be antiaromatic with four π electrons. For the sake of completeness, we discuss some aspects of the bonding in this cluster. The cluster, as discussed earlier, is composed of two Al_2Li_2 units arranged edge-to-edge to form an Al_4 rectangle. In this cluster, sp^2 hybridization of Al takes place leaving one empty unhybridized *p* orbital. The valence electron of each of the four Li atoms is then transferred to the empty p_z orbital, thus providing four π electrons for antiaromaticity. Havenith *et al.* [20], however, showed that the magnetic-field-induced *ring currents* exhibit a mixed character with competing diatropic and paratropic subpatterns. They also concluded that the concept of aromaticity and antiaromaticity should be extended to metal-atom clusters.

Our analysis indicates that the first low-energy structure above the lowest energy [Fig. 1(c), (2)] can also be considered a candidate for antiaromaticity. It has four π electrons similar to that of the lowest-energy structure, thereby conforming the structural and electron count criteria for antiaromaticity. A detailed analysis of the magnetic-field-induced ring currents has as yet not been done in order to conclude with confidence the antiaromaticity of this structure.

3. Al_5Li_5 and Al_6Li_8

As discussed in Sec. III A, the structures of Al_5Li_5 and Al_6Li_8 (in fcc geometry) clusters show a square-plane of Al_4.

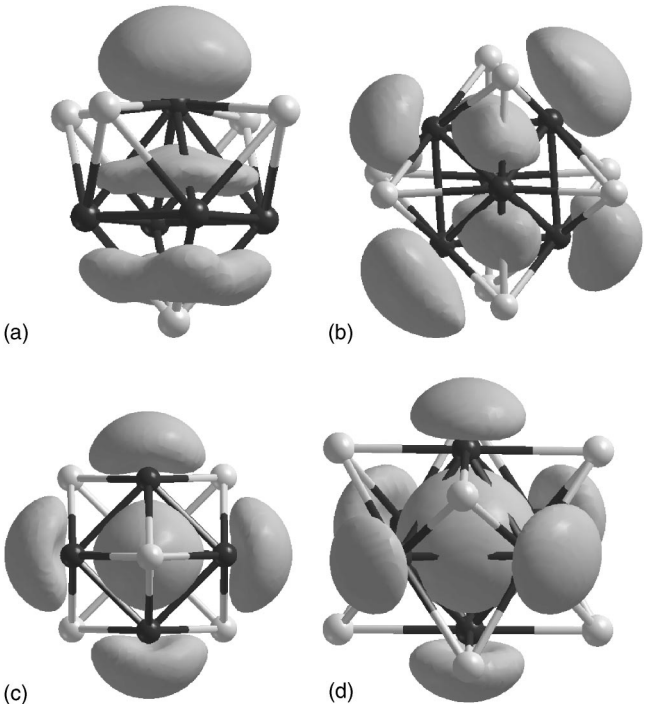

FIG. 6. (a) The isodensity surface of the HOMO of Al_5Li_5 at one-fifth of its maximum. (b) The isodensity surface of the HOMO of Al_6Li_8 at one-fifth of its maximum. (c) The isodensity surface of the sixth orbital of Al_5Li_5 at one-fifth of its maximum. (d) The isodensity surface of the tenth orbital of Al_6Li_8 at one-eighth of its maximum. In all of the figures, the black circles represent Al atoms and the gray circles represent Li atoms.

Such an Al_4 square-plane in Al_4^{2-} and Li-Al_4^- has led to aromaticity in these clusters [17]. Moreover, these clusters (Al_4^{2-}, Li-Al_4^-, Al_5Li_5, and Al_6Li_8) show a three-dimensional octahedral growth of the Al cluster. It is therefore interesting to discuss the change in bonding, and the effect on aromaticity in these clusters. We recall that Al_4^{2-} and Li-Al_4^- are aromatic clusters with two π electrons [17]. The HOMOs of these clusters are completely delocalized π orbitals. There are two more delocalized σ bonds: one is composed of radial *p* orbitals which lie along the diagonal of the square of Al_4 structure, and the other is composed of *p* orbitals perpendicular to the diagonal. These orbitals are referred to as radial and perpendicular orbitals by Wang and co-workers in Ref. [21]. Due to the presence of an Al_4 square-plane, the bonding in Al_5Li_5 and Al_6Li_8 clusters is expected to be similar to that in Al_4^{2-}. In that case, these clusters would have two π electrons, and provide partial evidence of aromaticity. In Figs. 6(a) and 6(b), we show the HOMO of Al_5Li_5 and Al_6Li_8. Interestingly, the HOMO of Al_5Li_5 does show such a delocalized π bond between the Al atoms in the Al_4 square [Fig. 6(a)]. However, a single electron is seen at the fifth Al atom that caps this square. This reduces the number of π electrons to one, thereby losing the aromaticity. The HOMO of Al_6Li_8, on the other hand, is quite different from that seen for the Al_5Li_5 cluster [see Fig. 6(b)]. It shows a localized bond composed of *p* orbitals of the Al atoms. We have also shown, in Figs. 6(c) and 6(d), the isodensity surfaces of the sixth orbital of Al_5Li_5 and the tenth orbital of Al_6Li_8, respectively.

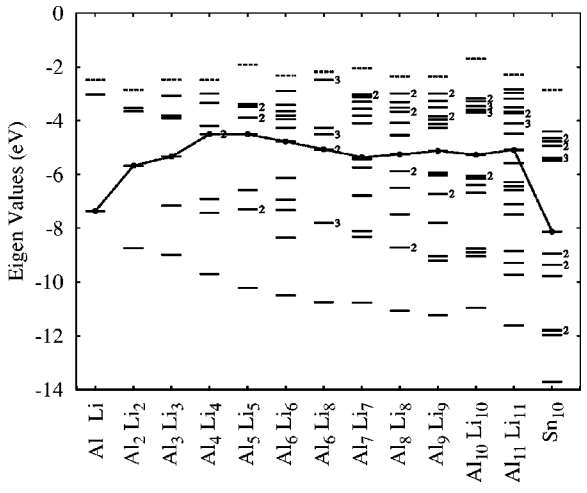

FIG. 7. The eigenvalue spectrum (in eV) of Al_nLi_n ($n=1-11$), Al_6Li_8, and Sn_{10} clusters. The continuous lines correspond to the occupied orbitals and the dotted lines correspond to the empty orbitals. The numbers on the right indicate the degeneracy of the orbitals. All orbitals are doubly occupied. The thick dashed line shows the *n*th orbital of these clusters, where *n* is the number of Al atoms. For Sn_{10}, the thick dashed line corresponds to the tenth orbital.

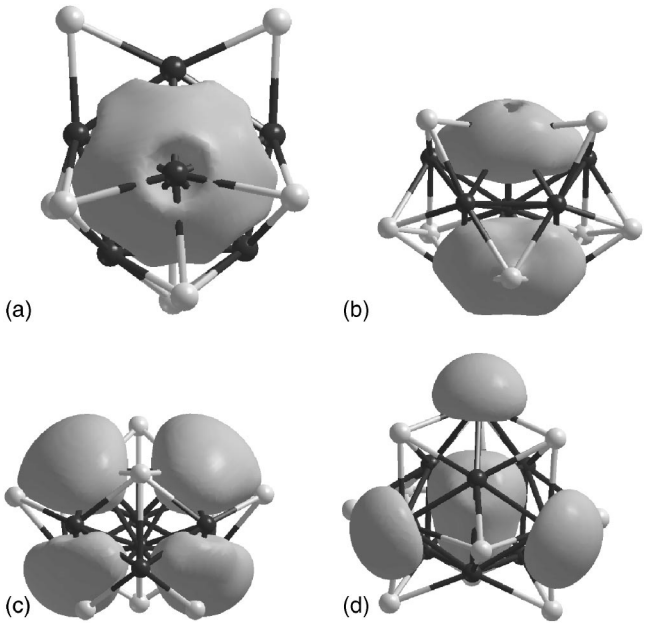

FIG. 8. The isodensity surface of various orbitals. These are (a) first orbital of Al_7Li_7 at one-fifth of its maximum value, (b) third orbital of Al_8Li_8 at one-fifth of its maximum value, (c) eighth orbital of Al_9Li_9 at one-tenth of its maximum value, and (d) tenth orbital of $Al_{10}Li_{10}$ at one-fifth of its maximum value, representing the 1*s*, 1*p*, 1*d*, and 2*s* orbital of the jellium formed out of the Al 3*s* orbital. In all of the figures, the black circles represent Al atoms and the gray circles represent Li atoms.

These are σ-type bonds, composed of radial *p* orbitals, and are analogous to the radial *p* orbitals of Al_4^{2-}, as noted by Wang *et al.* [21]. Since these bonds involve all the Al atoms, they exhibit a substantial delocalization.

In Fig. 7, we show the eigenvalue spectrum of Al_6Li_8, along with that of Al_nLi_n ($n=1-11$) and Sn_{10} clusters. It is clear from this plot that the eigenvalue spectrum of Al_6Li_8 shows a structure which is similar to the structure given by the jellium model. However, an analysis of the behavior of the molecular orbitals (figure not shown) of Al_6Li_8 shows that the lower six orbitals are jelliumlike, whereas the higher-energy orbitals form localized bonds arising out of *p* orbitals of the Al atoms.

4. Al_nLi_n(n=7-11)

The bonding in these clusters (Al_nLi_n, $n=7-11$) is quite different from that of the smaller clusters. Analysis of the behavior of the MOs and the eigenvalue spectrum shows that the spectrum can be classified into two parts: a lower-energy group consisting of jelliumlike orbitals and a higher-energy group consisting of localized bonds arising out of the interaction of the *p* electrons of each of the Al atoms. The number of orbitals in the lower group is *n*, where *n* is the number of Al atom in Al_nLi_n. Thus, the number *n* happens to be the demarcation number between the two sets, as shown in Fig. 7. The lower orbitals may be identified as $1s, 1p, 1d, 2s\ldots$, in conformation to the SJM. Typical isodensity plots of these orbitals are shown in Fig. 8 which represent the 1*s*, 1*p*, 1*d*, and 2*s* orbitals of the jellium model. In Fig. 7, we show the eigenvalue spectrum of Al_nLi_n($n=1-11$) and Sn_{10} clusters. The figure shows a clear energy separation of lower jelliumlike *n* orbitals of the clusters with $n>6$ from the higher-energy orbitals. In order to study this in more detail, we have performed a spherical harmonics analysis of the KS orbitals [44]. We find that the lower *n* orbitals have a predominant *s*-like character (75–85%) indicating that these orbitals are arising out of the 3*s* orbitals of the Al atoms. The higher-energy orbitals, composed of atomic Al 3*p* orbitals, give rise to localized bonds.

5. ELF in Al_nLi_n clusters

The localization characteristics in the bonding in the Al -Li clusters is also analyzed via the electron localization function plots. Previous investigations show that even in large Al-Li clusters, the Al-Al bond is covalent. However, our earlier work [29–31] as well as the present work show a clustering of Al atoms the inside Li cage. This clustering could lead to a delocalization of the electron density. In order to study this, we have analyzed the electron localization function in the Al_nLi_n clusters. In Fig. 9, we show the isovalued surfaces of the ELF for the clusters Al_2Li_2, Al_5Li_5, and $Al_{10}Li_{10}$, at values corresponding to 0.85, 0.8, and 0.72, respectively. These plots show a localization of the electron density along the Al-Al bond (increasing the value of ELFs does not show any bond between Al-Al). It has been noted by Silvi *et al.* [32] that an ELF value of about 0.7 or greater is an indication of a localized bond in that region. Thus, the Al-Al bonds in these clusters are predominantly covalent, in accordance with the earlier observation. However, as the cluster grows in size, the degree of localization of the electron density is reduced. Further, the localization in Al_5Li_5 is only in the plane forming the square (for out of plane, the

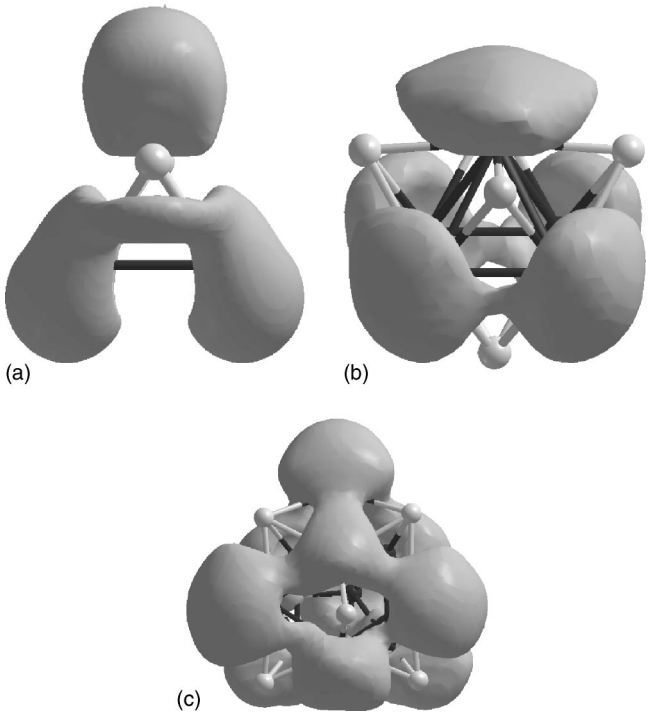

FIG. 9. The isodensity surface of the electron localization function (ELF) of (a) Al_2Li_2 at the value 0.85, (b) Al_5Li_5 at the value 0.80, and (c) $Al_{10}Li_{10}$ at the value 0.72. In all of the figures, the black circles represent Al atoms and the gray circles represent Li atoms.

Al-Al bond is seen with an ELF value of 0.7). A similar behavior of the ELF for Al_7Li_7 (not shown in the figure) is also seen. It has a localized bond along the pentagon (ELF value =0.78) and a delocalized bond in the direction perpendicular to the plane of the pentagon (ELF value =0.6).

IV. TETRAVALENT BEHAVIOR OF Al IN Al_nLi_n CLUSTERS

Previous investigations on mixed Al-Li clusters [15,45,46] have shown a substantial charge transfer from the Li atom to the Al atom. Due to the transfer, Al behaves as a tetravalent atom in mixed Al-Li clusters having nearly 50:50% concentration. In this section, we present the evidence of such behavior. The analysis of the geometries of Al_n in Al_nLi_n shows remarkable similarities to those of the clusters of the tetravalent atoms such as Si, Ge, Sn, and Pb. The transition from planar to three-dimensional geometry at $n=5$, the appearance of a pentagonal ring at $n=7$, and the formation of the distorted TTP structure at $n=10$ match with some of the features of the clusters of tetravalent atoms. Moreover, the eigenvalue spectrum of $Al_{10}Li_{10}$ (Fig. 7) shows a remarkable similarity to that of the Sn_{10} cluster. The bonding between Al-Al in these clusters is covalent, which is similar to that in the clusters of tetravalent atoms. Finally, the resemblance of the DOS of the Al-Li in its most stable bulk phase, i.e., B32, to that of diamond [25] also indicates a tetravalent behavior of the Al atom in Al-Li systems.

V. CONCLUSION

We have reported in this paper the geometries, energies, electronic structure, and bonding in various Al-Li clusters, viz., $Al_nLi_n(n=1-11)$, Al_2^-, Al_2^{2-}, Al_2Li, Al_2Li^-, and Al_6Li_8 using Born-Oppenheimer molecular dynamics within the framework of density-functional theory. The bonding in these clusters was discussed via the electron localization function as well as the behavior of the molecular orbitals. The growth pattern is divided into two broad categories, the first consisting of a bent rhombus ($n=2-4$) and the second consisting of a pentagonal ring ($n=7-9,11$). We find the 8-, 20-, and 40-valence-electron systems to be magic, exhibiting a peak in the dissociation energy, a minimum in the second difference in energy, and a large HOMO-LUMO gap. The structural transition of Al_n in Al_nLi_n from two dimensions to three dimensions increases the surface area, thereby allowing the Li atoms to maximize the number of Al-Li bonds, as a result of which the Li atoms move closer to the Al atoms. A substantial charge transfer from the Li atoms to the Al atoms is observed in nearly all the clusters, with the exception of Al_2Li_2. In this cluster, a hybridization of the 2*s* orbital of Li with the 3*p* orbital of Al takes place. In clusters with more than six Al atoms, the charge transfer makes Al behave as a tetravalent atom such as Si, Ge, Sn, and Pb in Al_nLi_n clusters. The negatively charged Al_n structure is then stabilized by the positively charged Li environment. The behavior of the molecular orbitals in these clusters ($n>6$) can be divided into two groups: a lower-energy group of jelliumlike orbitals arising out of the 3*s* electrons of the Al atoms and a higher-energy group of localized bonds formed through the interaction of the 3*p* electrons on each of the Al atoms. The formation of the three-dimensional Al_n structure destroys the aromatic and antiaromatic nature in these clusters.

ACKNOWLEDGMENTS

S.C. gratefully acknowledges the financial support of CSIR (New Delhi). V.V.P. wishes to thank NSERC of Canada and the University of Pune for partially supporting this research. We thank Dr. Sourav Pal for helping us to prepare the manuscript.

[1] H. W. Kroto, J. R. Heath, S. C. O'Brian, R. F. Curl, and R. E. Smalley, Nature (London) **318**, 162 (1985).

[2] W. D. Knight, K. Clemenger, W. A. de Heer, W. A. Saunders, M. Y. Chou, and M. I. Cohen, Phys. Rev. Lett. **52**, 2141 (1984).

[3] M. Schmidt, R. Kushe, W. Kronmüller, B. von Issendorff, and H. Haberland, Nature (London) **393**, 238 (1998); Phys. Rev. Lett. **79**, 99 (1997).

[4] A. A. Shvartsburg and M. F. Jarrold, Phys. Rev. Lett. **85**, 2530 (2000).

[5] Vijay Kumar, K. Esfarjini, and Y. Kawazoe, *Advances in Cluster Science* (Springer-Verlag, Heidelberg, 2000); *Theory of Atomic and Molecular Clusters with a Glimpse at Experiments*, edited by J. Jellinek, Springer Series in Cluster Physics (Springer, Berlin, 1999); *Physics and Chemistry of Finite Systems: From Clusters to Crystals*, edited by P. Jena, S. N. Khanna, and B. K. Rao (Kluwer Academic, Dordrecht, The Netherlands, 1992).

[6] P. Jena and S. N. Behera, *Clusters and Nanostructured Materials* (Nova Science Publishers, Inc., New York, 1996).

[7] *Reviews of Modern Quantum Chemistry*, edited by K. D. Sen (World Scientific, Singapore, 2002), Vols. I and II.

[8] M. C. Payne, M. P. Teter, D. C. Allan, T. A. Arias, and J. D. Joannopoulos, Rev. Mod. Phys. **64**, 1045 (1992).

[9] I. Boustani, W. Pewerstorf, P. Fantucci, V. Bonačić-Koutecký, and J. Koutecký, Phys. Rev. B **35**, 9437 (1987).

[10] B. K. Rao and P. Jena, J. Chem. Phys. **111**, 1890 (1999).

[11] B. K. Rao and P. Jena, J. Chem. Phys. **113**, 1508 (2000).

[12] Ajeeta Dhavale, D. G. Kanhere, S. A. Blundell, and R. Zope, Phys. Rev. B **65**, 085402 (2002).

[13] Hai-Ping Cheng, R. N. Barnett, and Uzi Landman, Phys. Rev. B **48**, 1820 (1993).

[14] Jaakko Akola and Matti Manninen, Phys. Rev. B **65**, 245424 (2002).

[15] Vijay Kumar, Phys. Rev. B **60**, 2916 (1999).

[16] X. Li, H. Wu, X.-B. Wang, and L.-S. Wang, Phys. Rev. Lett. **81**, 1909 (1998).

[17] Xi Li, Aleksey E. Kuznetsov, Hai-Feng Zhang, Alexander I. Boldyrev, and Lai-Sheng Wang, Science **291**, 859 (2001); Xi Li, Hai-Feng Zhang, Lai-Sheng Wang, Aleksey E. Kuznetsov, Nathan A. Cannon, and Alexander I. Boldyrev, Angew. Chem., Int. Ed. **40**, 1867 (2001).

[18] The antiaromatic properties in Al_4Li_4 were presented in the *Abstract in the Symposium on Trends in Theoretical Chemistry–2002 (TTC-2002)* (Indian Association for the Cultivation of Science, Kolkata, 2003).

[19] S. Shetty, D. G. Kanhere, and S. Pal, J. Phys. Chem. A **108**, 628 (2004).

[20] Remco W. A. Havenith, Patrick W. Fowler, Erich Steiner, Sharan Shetty, Dilip Kanhere, and Sourav Pal, Phys. Chem. Chem. Phys. **6**, 285 (2004).

[21] Aleksey E. Kuznetsov, K. Alexander Birch, Alexander I. Boldyrev, Xi Li, Hua-Jin Zhai, and Lai-Sheng Wang, Science **300**, 622 (2003).

[22] Molecules that are cyclic, planar, conjugated, possessing $(4n+2)\pi$ electrons, and having chemical and structural stability are called aromatic molecules. For details, see the special issue on aromaticity, Chem. Rev. (Washington, D.C.) **101** (5) (2001).

[23] R. Breslow and W. Chu, J. Am. Chem. Soc. **92**, 2165 (1970); R. Breslow, Acc. Chem. Res. **6**, 393 (1973).

[24] X.-Q. Guo, R. Podloucky, and A. J. Freeman, Phys. Rev. B **40**, 2793 (1989); Phys. Rev. B **42**, 10 912 (1990).

[25] A. Arya, G. P. Das, H. G. Salunke, and S. Banerjee, J. Phys.: Condens. Matter **6**, 3389 (1994).

[26] D. Tomanek and M. A. Schlüter, Phys. Rev. Lett. **56**, 1055 (1986); P. Ballone, W. Andreoni, R. Car, and M. Parrinello, *ibid.* **60**, 271 (1988); K. Raghavchari and C. M. Rohlfing, J. Chem. Phys. **89**, 2219 (1988); I. Vasiliev, S. Ögüt, and J. R. Chelikowsky, Phys. Rev. Lett. **78**, 4805 (1997).

[27] S. Ögüt and J. R. Chelikowsky, Phys. Rev. Lett. **56**, 2656 (1986).

[28] Bing Wang, L. M. Molina, M. J. Lo'pez, A. Rubio, J. A. Alonso, and M. J. Stott, Ann. Phys. (Leipzig) **7**, 107 (1998).

[29] Vaishali Shah, D. G. Kanhere, Chiranjib Majumder, and G. P. Das, J. Phys.: Condens. Matter **9**, 2165 (1997).

[30] V. Shah and D. G. Kanhere, J. Phys.: Condens. Matter **8**, L253 (1997).

[31] A. M. Vichare and D. G. Kanhere, Eur. Phys. J. D **4**, 89 (1998).

[32] B. Silvi and A. Savin, Nature (London) **371**, 683 (1994).

[33] W. Kohn and L. J. Sham, Phys. Rev. Lett. **140**, A1133 (1965).

[34] M. C. Payne, J. D. Joannopoulos, D. C. Allan, M. P. Teter, and D. H. Vanderbilt, Phys. Rev. Lett. **56**, 2656 (1986).

[35] G. B. Bachelet, D. R. Hamann, and M. Schlüter, Phys. Rev. B **26**, 4199 (1982).

[36] L. Kleinman and D. M. Bylander, Phys. Rev. Lett. **48**, 1425 (1982).

[37] D. M. Ceperley and B. J. Alder, Phys. Rev. Lett. **45**, 566 (1980); J. P. Perdew and A. Zunger, Phys. Rev. B **23**, 5048 (1981).

[38] D. Vanderbilt, Phys. Rev. B **41**, 7892 (1990).

[39] Vienna *Ab initio* Simulation Package (VASP), Technishe Universität, Wien, 1999.

[40] J. P. Perdew and Y. Wang, J. Chem. Phys. **45**, 13244 (1992).

[41] S. Chacko, M. Deshpande, and D. G. Kanhere, Phys. Rev. B **64**, 115409 (2001).

[42] U. Röthlishberger, W. Andreoni, and P. Giannozzi, J. Chem. Phys. **96**, 1248 (1992).

[43] Kavita Joshi, D. G. Kanhere, and S. A. Blundell, Phys. Rev. B **66**, 155329 (2002).

[44] The character in an orbital is calculated by projecting the orbital onto spherical harmonics centered at each ionic site within a sphere of a specified radius around each ion. The radius of the sphere is taken to be half of the distance of the ion from the nearest ion.

[45] X. G. Gong and V. Kumar, Phys. Rev. Lett. **70**, 2078 (1993).

[46] X. G. Gong and V. Kumar, Phys. Rev. B **50**, 17701 (1994).